Some Two-Layer Models of the Shelf–Slope Front: Geostrophic Adjustment and its Maintenance[1]

HSIEN WANG OU

Lamont–Doherty Geological Observatory of Columbia University, Palisades, N.Y. 10964

(Manuscript received 17 November 1982, in final form 23 May 1983)

ABSTRACT

Two conceptual models of a two-layered frontal system are presented to study the wintertime shelf–slope front. The first model examines the geostrophic adjustment over a step topography after the fall overturning and applies only over short time scales before the nonconservative processes become important. The second model, on the other hand, examines the thermodynamic balance over longer time scales when some dissipative and mixing effects are included.

From the geostrophic-adjustment model, it is found that the flat-bottom solution of a less-dense shelf water with respect to the slope water is little modified by the presence of a step. But in the case of denser shelf water, the solution shows the detachment of the spillage when the depth ratio across the step is greater than two, resembling some regional observations.

In the frictional model, the wind generated entrainment is demonstrated to provide a virtual momentum source to maintain the along-front current shear against friction and thus can account for the persistence of the front through the winter season. The entrainment also decreases the buoyancy of the exported shelf water, the distribution of which however, varies greatly with the external parameters. For parameter values applicable to the Middle Atlantic Bight, an inflection point, corresponding to a weakened lateral buoyancy gradient, is predicted above the front, consistent with observation.

1. Introduction

In the Middle Atlantic Bight, a seasonal thermocline dominates the hydrography during summer months. In late fall, overturning events, triggered by increased wind stirring and surface cooling, break down the seasonal thermocline and mix the shelf water which, on account of its relative freshness, constitutes a lighter water mass than the slope water. The transition between the two is generally abrupt, hence the term shelf–slope front, and occurs near the shelf break (see Fig. 1). If the overturning is a sudden event, then immediately afterwards the isopycnals are vertical, accompanied by little mean fluid motion. This is a dynamically unbalanced state, and the gravitational flow generated, whereby the lighter shelf water flows seaward above the shoreward flowing slope water will induce a vertical shear in the along-front current until geostrophic balance is restored and the front achieves equilibrium.

Assuming that the adjustment process is inviscid so that the potential vorticity is conserved, a number of researchers (e.g., Csanady, 1971; Stommel and Veronis, 1980) have solved the equilibrium state of a two-layered frontal system overlying a flat bottom. Since it is the rapid depth change that facilitates the formation of the front near the shelf break, it is important to examine the topographic effect on their solutions. In this pursuit, Hsueh and Cushman-Roisin (1982) have recently solved the problem numerically over a topography of two adjoining linear slopes. Our first model (Section 2) represents a simplification of their work by employing a step topography and rigid lid. The simplification allows for an analytical solution and hence a more ready examination of its properties, and is still adequate to assess the lowest-order effect of the shelf break. We also present solutions for the cases of dense shelf water and a narrow shelf that might have regional applications.

The inertial adjustment model obviously breaks down over longer time periods when nonconservative processes become important. In particular, friction dissipates the current shear and flattens the front, and mixing reduces the density contrast across the frontal interface; both tend to destroy the shelf–slope front. But since the front is observed to persist through the winter season, as evidenced by the March observations shown in Fig. 1, then there must exist some momentum and buoyancy source for its maintenance. This is the subject of our second model (Section 3) where a steady state balance is proposed that includes some dissipative and mixing effects.

[1] Lamont–Doherty Geological Observatory Contribution No. 3530.

© 1983 American Meteorological Society

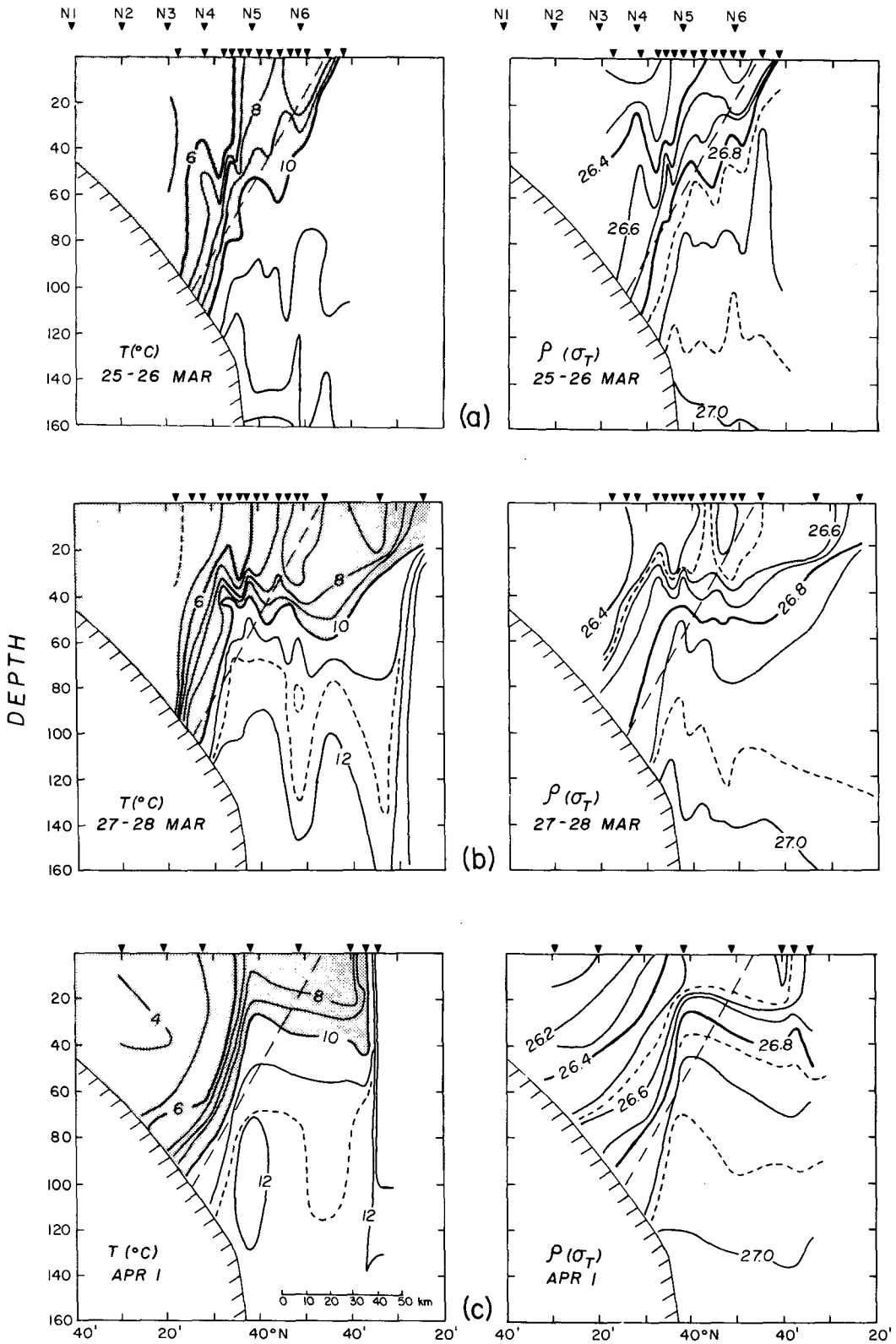

FIG. 1. Temperature and density sections across the New England shelf-slope front (adapted from Marra *et al.*, 1982).

Evaluations of the models are presented in both sections, with major conclusions summarized in Section 4.

2. Geostrophic adjustment

a. Governing equations

Figure 2 shows the model geometry where the front is a two-dimensional interface (in the y–z plane) that separates two homogeneous layers and overlies a step topography. Initially, the front is a vertical interface located at the step, shown by the dashed line, and the fluid is motionless. The model seeks to determine the equilibrium front, shown schematically by the solid line, after the geostrophic adjustment. The adjustment process is assumed inviscid and adiabatic so that the potential vorticity is conserved, and the frontal interface remains material. In our terminology, the upper and lower layers are labeled 1 and 2, and the x and y directions are called along- and cross-frontal respectively. All field variables in the lower case refer to the adjusted state.

For conciseness, the following derivations are based on dimensionless variables. We have scaled the vertical and horizontal coordinates by, respectively, the shelf depth (H_1) and the internal radius of deformation (λ) based on this depth, defined as $(g'H_1)^{1/2} f^{-1}$ where g' is the reduced gravity and f is the Coriolis parameter. We have chosen $f\lambda$ as the velocity scale.

Conservation of potential vorticity states that

$$\left.\begin{aligned} 1 - u_{1y} &= h_1 \\ 1 - u_{2y} &= h_2\delta^{-1} \end{aligned}\right\}, \tag{2.1}$$

where $\delta \equiv H_2/H_1$ is the depth ratio across the step and the subscript y represents differentiation. Since the front is material, it does not allow any transverse motion in the adjusted state, the along-front current must then be geostrophic and satisfy the Margules equation,

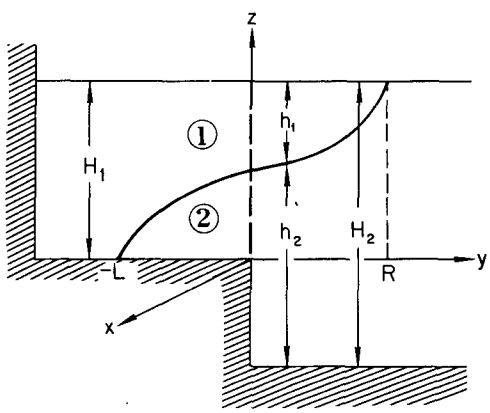

FIG. 2. A simplified frontal system used in the geostrophic adjustment model. The dashed and solid line represent the front in its initial and adjusted state, respectively.

$$u_1 - u_2 = -h_{1y}. \tag{2.2}$$

Stommel and Veronis (1980) have shown that allowing a free surface has little effect on the frontal shape; we will therefore assume a rigid lid so that

$$h_1 + h_2 = H \equiv \begin{cases} 1, & y < 0 \\ \delta, & y > 0. \end{cases} \tag{2.3}$$

Combined with (2.1) and (2.2), a single equation in h_1 can be derived,

$$h_{1yy} - \gamma^2 h_1 = -H/\delta, \tag{2.4}$$

where $\gamma^2 \equiv 1 + \delta^{-1}$.

To derive the boundary condition at $y = -L$ where the front intersects the bottom, we first integrate the x-momentum equation in time to give

$$\left.\begin{aligned} u_1 &= y - \eta_1 \\ u_2 &= y - \eta_2 \end{aligned}\right\}, \tag{2.5}$$

where η_1 and η_2 are the initial positions of the water column presently at y. Invoking the implicit presence of a distinct coast, the rigid-lid assumption requires that the net cross-shelf mass flux vanishes. This leads to

$$\eta_1 = -L,\ \eta_2 = 0 \quad \text{at} \quad y = -L \tag{2.6}$$

which translates, through (2.5) and (2.2), to

$$h_{1y} = -L \quad \text{at} \quad y = -L. \tag{2.7}$$

Similarly, where the front intersects the top surface, we have

$$h_{1y} = -R \quad \text{at} \quad y = R. \tag{2.8}$$

Together with the boundary condition that

$$h_1 = \begin{cases} 1 & \text{at} \quad y = -L \\ 0 & \text{at} \quad y = R, \end{cases} \tag{2.9}$$

and the matching condition that

$$h_1,\ h_{1y} \text{ be continuous at } y = 0, \tag{2.10}$$

Eq. (2.4) can be solved. The matching condition that h_{1y} be continuous is equivalent to the condition that η_1 and η_2 be continuous, as can be easily seen from (2.2) and (2.5).

b. The solution

Eq. (2.4) has the general solution,

$$\left.\begin{aligned} h_1 &= A\cosh\gamma y + B\sinh\gamma y + \frac{1}{\gamma^2\delta} \\ &\qquad \text{for} \quad y \leqslant 0 \\ h_1 &= \bar{A}\cosh\gamma y + \bar{B}\sinh\gamma y + \frac{1}{\gamma^2} \\ &\qquad \text{for} \quad y \geqslant 0 \end{aligned}\right\}, \tag{2.11}$$

where A, B, $\bar{A}$, $\bar{B}$ are constants yet to be determined.

The boundary and matching conditions, (2.7) to (2.10), lead to

$$A \sinh\gamma L - B \cosh\gamma L = \frac{\gamma L}{\gamma^2}, \tag{2.12}$$

$$\bar{A} \sinh\gamma R + \bar{B} \cosh\gamma R = -\frac{\gamma R}{\gamma^2}, \tag{2.13}$$

$$A \cosh\gamma L - B \sinh\gamma L = \frac{1}{\gamma^2}, \tag{2.14}$$

$$\bar{A} \cosh\gamma R + \bar{B} \sinh\gamma R = -\frac{1}{\gamma^2}, \tag{2.15}$$

$$\bar{A} = A + \frac{1}{\gamma^2}\left(\frac{1}{\delta} - 1\right), \tag{2.16}$$

$$\bar{B} = B. \tag{2.17}$$

These six algebraic equations can be solved for the six unknown constants (A, B, $\bar{A}$, $\bar{B}$, L, R) to give (see Appendix A)

$$\left.\begin{aligned} \bar{A} &= -A = \frac{1}{2\gamma^2}\left(\frac{1}{\delta} - 1\right) \\ \bar{B} &= B = \frac{1}{\gamma^2}(\sinh\gamma L - \gamma L \cosh\gamma L) \\ L &= R \\ \cosh\gamma L - \gamma L \sinh\gamma L &= \frac{1}{2}\left(1 - \frac{1}{\delta}\right) \end{aligned}\right\}. \tag{2.18}$$

Since $\bar{A} = -A$ and $\bar{B} = B$, it follows from (2.11) that

$$h_1(y) + h_1(-y) = 1, \tag{2.19}$$

and hence, with the boundary condition (2.10),

$$h_1(0) = \tfrac{1}{2}, \tag{2.20}$$

regardless of the value of δ. It is interesting to note this symmetry property although the topography can be highly asymmetric.

The solutions for the case of $\delta = 1$ and 10 are plotted in solid lines in Fig. 3. It is seen that the flat-bottom solution is little modified by the step topography. The frontal zone is slightly widened, but its half-width is still roughly given by the internal radius of deformation based on the shelf depth. This is expected as the upper layer has a greater potential vorticity and dominates the vorticity balance.

Since the value of δ has not been restricted, the above solution also applies to the case of $\delta < 1$ when the shelf water is the denser of the two. The equality (2.20) however limits the depth ratio to greater than ½ or the front would cut through a solid boundary, an obviously erroneous solution. The only boundary condition that can be relaxed when $\delta < \frac{1}{2}$ is the requirement that h_1 be continuous at the step; in other words, the spillage of the dense shelf water must be allowed to detach from its source region. Setting $h_1 = \delta$ at $y = 0^+$, (2.16) is replaced by

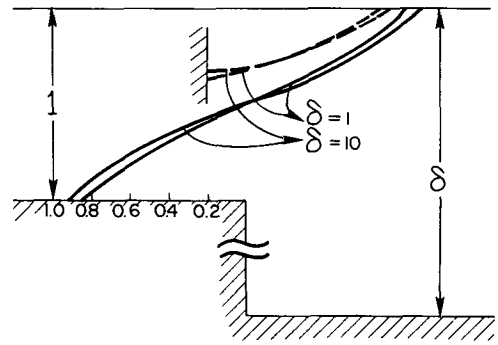

FIG. 3. Geostrophically adjusted front for $\delta = 1$ and 10. Solution for a wide shelf is shown in solid lines, and that for a narrow shelf (with a shelf width equal to one-fifth the internal radius of deformation) is shown in dashed lines.

$$\bar{A} = \delta\gamma^{-2}. \tag{2.21}$$

The remaining constants can be solved for to give (see Appendix A)

$$\left.\begin{aligned} A &= -\bar{A} = -\frac{\delta}{\gamma^2} \\ \bar{B} &= B = \frac{1}{\gamma^2}(\sinh\gamma L - \gamma L \cosh\gamma L) \\ L &= R \\ \gamma L \sinh\gamma L - \cosh\gamma L &= \delta \end{aligned}\right\}. \tag{2.22}$$

The solution for the case $\delta = 0.1$ is shown in Fig. 4 by the solid line. The symmetry property (2.19) still holds and the detached parcel has a vertical extent given by the shelf depth. Since less vortex compression is experienced by the dense shelf water descending the step, the frontal zone is seen to be wider. There is considerable modification to the solution when a more realistic topography is used (Hsueh and Cushman-Roisin, 1982), but this qualitative feature remains unchanged.

The heavy solid line in Fig. 5 shows the half-width of the frontal zone as a function of the depth ratio δ. It has a minimum value of 0.8 at $\delta = 1$, and increases to the asymptotic value of 1.2 or 0.9 as δ approaches zero or infinity, respectively. Despite vastly different values of the depth ratio, the frontal width therefore remains nearly constant and is roughly given by the internal radius of deformation based on the shelf depth.

For completeness, we have also presented in Appendix B the solution for a narrow shelf when the equilibrium front intersects the coast. It is shown by the dashed lines in Figs. 3 and 4 when the shelf width is one-fifth the internal radius of deformation. The solution shown in Fig. 3 is a generalization of that of Griffiths and Linden (1982) where the lower layer

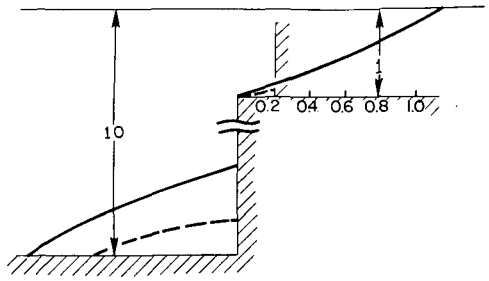

FIG. 4. As in Fig. 3, but for $\delta = 0.1$.

is assumed motionless. The coupling of the two layers increases the frontal slope and results in a narrower frontal zone. The contours of the maximum offshore displacement of the front are plotted as thin solid lines in Fig. 5 as a function of δ and the shelf width, denoted by L and R depending on whether δ is greater or smaller than 1. Except for very narrow shelves, this displacement is not a strong function of the shelf width and is again roughly given by the internal radius of deformation.

c. *Discussion*

There are obvious limitations of the model. Being inviscid and adiabatic, it applies only over short time scales before non-conservative processes become important. But even over inertial time scales, laboratory experiments (e.g., Griffiths and Linden, 1982) show that the front oscillates and meanders and frequently becomes unstable. The condition of two-dimensionality and steady state can be met only after proper spatial and temporal averages are taken, which places a stringent requirement on the data. Hydrographic surveys are not efficient for pinning down overturning events or for providing a temporal mean. Moored measurements, on the other hand, usually lack the spatial resolution to delineate the front which, making matters worse, moves about. Until adequate data can be obtained to compare with the model, the importance of geostrophic adjustment in shaping the shelf–slope front remains an open question.

The assumption of a sudden overturning that creates an initially vertical interface and motionless fluid has not been substantiated by observation. In fact, measurements from a string of four temperature sensors reported by Mayer, Hansen and Ortman (1979, their Fig. 14) suggest rather a gradual deepening and erosion of the seasonal thermocline. While there might be occasions of sudden overturning, their observation certainly casts some doubt on the application of the present model.

The detachment of the outspilled dense shelf water from its source region is one interesting feature predicted by the model. Although it resembles observations taken near the Weddell Sea (Foster and Carmack, 1976) and Ross Sea (Jacobs, Amos and Bruchhausen, 1970) shelf breaks, and near the Red Sea outflow (Wyrtki, 1971, p. 466), other processes, perhaps frictional in nature, cannot be ruled out as being responsible.

3. An entrainment model

a. *The governing equations*

As is evident from Fig. 1, the shelf–slope front is highly variable in time. But despite the transients, the front is observed to persist throughout the winter season. This persistence allows a definition of the mean front, the balance of which we are addressing here in this steady state model. Wind undoubtedly causes much of the frontal variability, but besides bodily displacing or deforming the front, it also generates turbulence which will be tacitly assumed in the model to mix the fluid vertically within layers, maintain a sharp frontal interface, and entrain fluid upward across this interface. The downward entrainment induced by bottom turbulence will be neglected because of the dominance of the turbulence from above.

The model configuration is shown in Fig. 6, where the front is again approximated by an interface adjoining fluids of different density. The density is vertically uniform within layers but allowed to vary horizontally. Along-front uniformity and steady state are assumed so that $\partial_x = \partial_t = 0$.

The entrainment rate is defined as

$$w_e = w_f + \frac{dh_1}{dt} = w_f + v_1 h_{1y}, \tag{3.1}$$

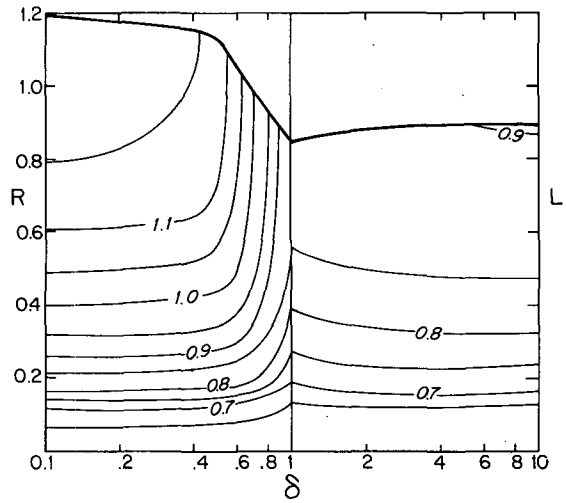

FIG. 5. Thick solid line is the half-width of the frontal zone for the case of a wide shelf, and thin solid lines are contours of the maximum offshore displacement of the front when the front intersects the coast. The shelf width is indicated by L (R) when δ is greater (smaller) than 1. All the distances have been scaled by internal radius of deformation based on the shallower depth.

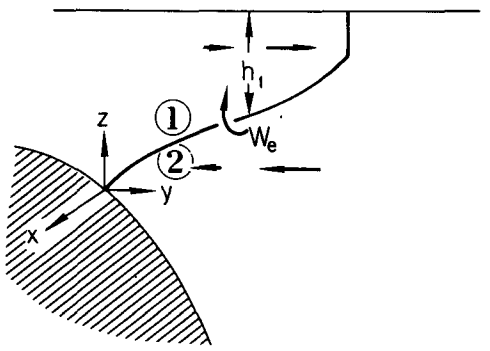

FIG. 6. A simplified frontal system used in the entrainment model.

where w_f is the vertical velocity at the front. Without mixing, the frontal interface is material so that $w_f = -dh/dt$, and w_e vanishes. But in the presence of upward entrainment, w_e is positive. By vertically integrating the continuity equation and assuming a rigid lid, we derive

$$w_f = h_1 v_{1y}, \tag{3.2}$$

which can be substituted into (3.1) to yield

$$V_{1y} = w_e, \tag{3.3}$$

where $V_1 \equiv h_1 v_1$ is the transport of the upper layer; mass conservation simply requires a transport divergence to accommodate the entrained fluid. Similarly, entropy conservation requires a divergence of the lateral density flux to accommodate the vertical density flux associated with the entrainment, or

$$(V_1\rho_1)_y = w_e\rho_2. \tag{3.4}$$

Similar equations apply to the lower layer,

$$V_{2y} = -w_e, \tag{3.5}$$

$$(V_2\rho_2)_y = -w_e\rho_2, \tag{3.6}$$

which lead however to

$$\rho_{2y} = 0, \tag{3.7}$$

or

$$\rho_2 = \text{constant}, \tag{3.8}$$

i.e., in the absence of downward entrainment, a fluid particle in the lower layer conserves its density which, in a steady state, must then be spatially uniform. Subject to this constraint, (3.3) and (3.4) imply that

$$(V_1\Delta\rho)_y = 0,$$

or

$$V_1\Delta\rho = \text{constant}, \tag{3.9}$$

where $\Delta\rho \equiv \rho_2 - \rho_1$ is the density difference across the frontal interface, the lateral flux of which is therefore a constant. Alternatively, mass and entropy conservation applying over the whole water column require that

$$(V_1 + V_2)_y = 0, \tag{3.10}$$

$$(V_1\rho_1 + V_2\rho_2)_y = 0, \tag{3.11}$$

which, subjected to the condition of a constant ρ_2, lead trivially to (3.9). A similar result has been derived by deSzoeke and Richman (1981) in their study of the upwelling front. If $V_1 = 0$ at $y = 0$, then according to (3.9), V_1 vanishes everywhere, contradicting (3.3); thus a steady state is possible only when there is a buoyancy influx at $y = 0$.

In the y-momentum equation, geostrophy is assumed so that

$$f\Delta u = -g\rho^{-1}\Delta\rho h_{1y}, \tag{3.12}$$

where Δu is the velocity jump across the interface and ρ, the mean density of the fluid, is assumed constant under the Boussinesq approximation. In the x-momentum equation, we assume that the Coriolis force acting on the offshore transport is balanced by the net of surface less interface stress,

$$-fV_1 = \tau\rho^{-1} - w_e\Delta u, \tag{3.13}$$

where τ is the surface wind stress and the interface stress has been parameterized in terms of the momentum flux associated with entrainment.

It is seen that the entrainment, although dissipative as a momentum flux, enhances the offshore transport through mass conservation (Eq. 3.3) which, when acted on by the Coriolis force, can maintain an along-front current shear against friction (Eq. 3.13). This somewhat peculiar mechanism of entrainment as a virtual momentum source works only in a rotating system and is the primary physical idea we are trying to convey here.

To close the problem, we parameterize the entrainment rate according to Kraus and Turner (1967),

$$w_e = \frac{2m_0u_*^3\rho}{g\Delta\rho h_1}, \tag{3.14}$$

where m_0 is some empirical constant of order 1 and u_* is the friction velocity defined by $(\tau^*/\rho)^{1/2}$ (τ^* being the magnitude of the turbulent wind stress).

If we scale $\Delta\rho$ and h_1 by their respective values at the origin y by the internal radius of deformation λ [defined here as $(g\rho^{-1}\Delta\rho(0)h_1(0))^{1/2}/f$], and $(\Delta u, V_1, w_e, \tau)$ by $(f\lambda, \lambda w_e^*, w_e^*, \rho f\lambda w_e^*)$ where w_e^* is the entrainment rate at $y = 0$, then, in terms of the dimensionless variables, the governing equations become

$$V_{1y} = w_e, \tag{3.15}$$

$$V_1\Delta\rho = F, \tag{3.16}$$

$$\Delta u = -\Delta\rho h_{1y}, \tag{3.17}$$

$$V_1 = w_e\Delta u - \tau, \tag{3.18}$$

$$w_e = 1/(h_1\Delta\rho), \tag{3.19}$$

where F, the transport at $y = 0$, and τ, the surface wind stress, are the only two external parameters of the system. The five equations thus determine the five variables ($\Delta\rho$, h_1, Δu, V_1, w_e) and the system is closed.

b. The solution

Eliminating all the variables in favor of h_1 and $\Delta\rho$, we derive

$$\frac{h_{1y}}{h_1} = -\frac{F}{\Delta\rho} - \tau, \tag{3.20}$$

$$\frac{1}{h_1} = -\frac{F}{\Delta\rho}(\Delta\rho)_y. \tag{3.21}$$

Multiplying the two and integrating the resulting equation, we obtain

$$\frac{1}{h_1} = 1 - F^2 + \frac{F^2}{\Delta\rho} - \tau F \ln\Delta\rho, \tag{3.22}$$

where the boundary condition that $h_1 = \Delta\rho = 1$ at $y = 0$ has been used. Substituting (3.22) into (3.21) yields

$$(\Delta\rho)_y = -\frac{1 - F^2}{F}\Delta\rho - F + \tau\Delta\rho \ln\Delta\rho \tag{3.23}$$

which can be integrated numerically.

For the purpose of our discussion, we will first examine the solution of vanishing τ, in which case the first integral of (3.23) gives

$$\Delta\rho = \frac{1}{1 - F^2}\{\exp[-y(1 - F^2)/F] - F^2\}, \tag{3.24}$$

with an accompanying gradient

$$(\Delta\rho)_y = -\frac{1}{F}\exp[-y(1 - F^2)/F]. \tag{3.25}$$

Except for the trivial case of $F = 1$ when this gradient is constant, its magnitude varies exponentially in y and is monotonically increasing or decreasing depending on whether F is greater or smaller than unity. We have plotted in Fig. 7 the solution for three different values of F (0.1, 1, and 10) which clearly shows this property. Physically, for a small shelf water export (i.e., a small F), its buoyancy is quickly reduced by the entrainment, resulting in a sharp gradient near the influx point. A larger shelf water export is however more apt to maintain its buoyancy against the entrainment effect, the lateral gradient of which is therefore small near the influx point and sharpens offshore as the entrainment rate increases. It is also trivial to show from (3.20) and (3.21), by setting $\tau = 0$, that

$$h_{1y} = \frac{1}{(\Delta\rho)_y}, \tag{3.26}$$

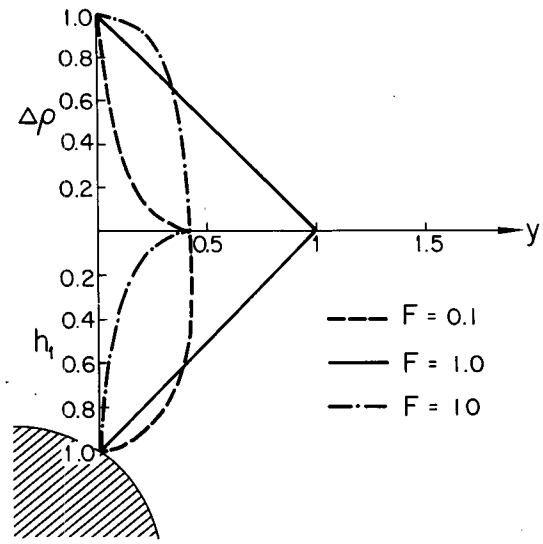

FIG. 7. Solution of $\Delta\rho$ and h_1 as a function of the offshore distance y for $\tau = 0$ and $F = 0.1$, 1, and 10.

i.e., the frontal slope is inversely proportional to the buoyancy gradient, as is clearly shown in Fig. 7. The frontal interface is therefore straight for $F = 1$, but is concave (convex) upward when F is greater (smaller) than one. Setting $\Delta\rho = 0$ in (3.24), one obtains the width of the frontal zone

$$y_f = -\frac{F}{1 - F^2}\ln F^2, \tag{3.27}$$

which has a maximum when $F = 1$. It is interesting to note that both large and small shelf water export lead to a narrower frontal zone.

c. The effect of a mean wind stress

The effect of wind stress on the buoyancy gradient can be inferred from the last term in (3.23). Since this term vanishes for $\Delta\rho = 1$ or 0, it has the maximum effect at some intermediate value of $\Delta\rho$ and, depending on the sign of τ, either sharpens or weakens the buoyancy gradient. It is possible then that an extremum can be generated in the buoyancy gradient (i.e. an inflection point) and it considerably modifies the solution shown in Fig. 7. In fact, the condition for inflection point (represented in the following by a superscript i)

$$\partial_y^2(\Delta\rho)^i = 0 \tag{3.28}$$

leads trivially to

$$(\Delta\rho)^i = \exp\left(\frac{1 - F^2}{F\tau} - 1\right), \tag{3.29}$$

the contours of which are plotted in Fig. 8. Since $\partial_y^3(\Delta\rho)^i\{=\tau[(\Delta\rho)_y^i]^2/(\Delta\rho)^i\}$ has the same sign as τ, the inflection point corresponds to a maximum (minimum) in the magnitude of the buoyancy gradient

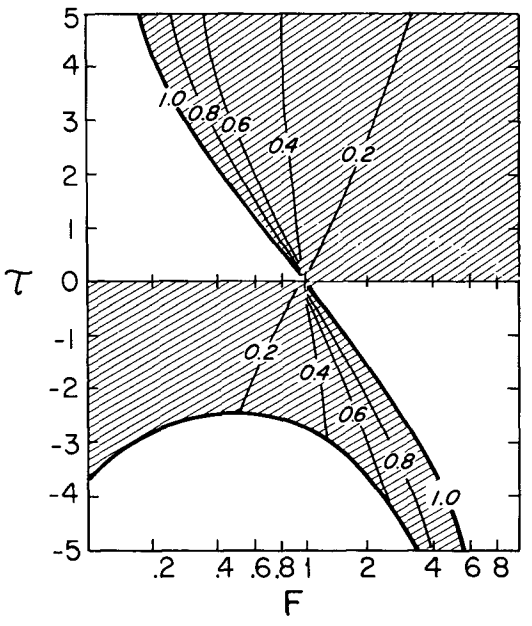

FIG. 8. Contours of $(\Delta\rho)^i$ as a function of F and τ. The lower solid curve represents $(\Delta\rho)^i_y = 0$ and the shaded areas indicate regions of inflection point.

when τ is positive (negative). For a negative wind, however, we must further require that $(\Delta\rho)^i_y$ never vanish, otherwise, (3.20) implies an infinite h_1 and an obvious breakdown of the model. The model therefore applies only above the lower curve shown in the figure representing $(\Delta\rho)^i_y = 0$, with shaded areas indicating regions of the inflection point. It is seen that for F of order 1 or less, there is a considerable range of negative wind stress that can generate an inflection point, resulting in a weakened buoyancy gradient at some mid-section above the front. This, as further substantiated by some parameter estimates later, can perhaps account for the observed frontal structure shown in Fig. 1.

The solutions for the case of $F = 1$ and $\tau = -2$, 0, and 2 are plotted in Fig. 9 which clearly show the inflection point predicted by Fig. 8. In addition, wind also modifies significantly the frontal shape. A positive wind generally drives a greater along-front current shear and steepens the front. A negative wind has just the opposite effect, but in this particular example of $\tau > F$, a negative along-front current shear is generated near $y = 0$ (see Eq. 3.18) and the frontal interface deepens offshore until the increasing offshore transport, replenished by entrainment, reverses the along-front current shear and the frontal slope. If the wind is strong enough, the frontal interface will deepen indefinitely, causing the breakdown of the model mentioned above. The shortcoming of the model can be remedied by the inclusion of some three-dimensional effects discussed in the next section.

d. Discussion

As remarked in Section 2.3, it is extremely difficult to derive a mean front from observations to compare with the model. Nor do we expect a model of this crudeness to apply in detail to the shelf–slope front, a phenomenon rich in both structure and physical processes. Our aim is to demonstrate that the entrainment can act as a viable mechanism for maintaining the front, thus accounting for its persistence. Some key hypotheses and qualitative features of the model nevertheless do compare favorably with observation, suggesting some validity for the proposed balance.

For example, the assumption of negligible downward entrainment leads to a structureless lower layer, consistent with the observations shown in Fig. 1. Despite the observed transients, the density field above the frontal interface exhibits sharper gradients at both the shoreward and seaward edge of the frontal zone, accountable by the model over certain parameter ranges. But do they correspond to realistic parameter values? The answer is affirmative according to the following estimates. Because of the great uncertainty involved, partly due to the imprecise definition of some parameters in a geophysical environment, only order of magnitude estimates will be attempted.

We use $\Delta\rho \approx 0.4 \times 10^{-3}$ and $h_1 \approx 100$ m as the buoyancy and depth scale. With $f \approx 10^{-4}$ s^{-1}, the internal radius of deformation is then 6 km. To estimate the scale of the entrainment rate (i.e., its value at $y = 0$), we set $m_0 \approx 0.5$ (Davis *et al.*, 1981) and $u_* \approx 2.2$ cm s^{-1} (corresponding to a 5 dyn cm^{-2} turbulent wind stress), which gives $w_e^* \approx 3$ m day^{-1}. The scales of the mean wind stress and the offshore transport are then 0.2 dyn cm^{-2} and 7 km^2 year^{-1} respectively.

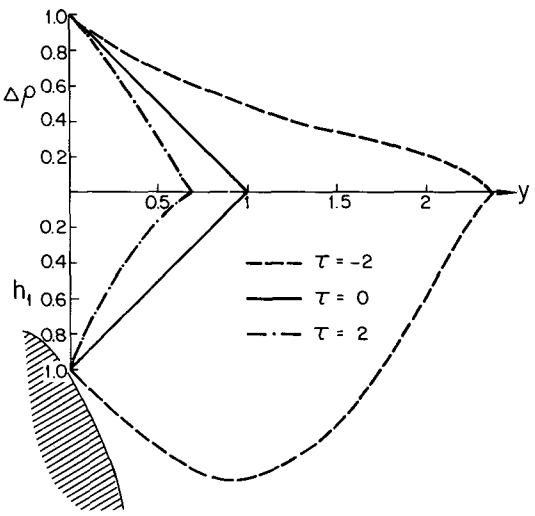

FIG. 9. Solution for the case $F = 1$ and $\tau = -2$, 0 and 2.

The mean wind stress, of course, varies from year to year, but in the Middle Atlantic Bight, it is generally negative and is given by the scale above (see, e.g., Beardsley and Boicourt, 1981). The offshore transport of shelf water is more difficult to determine. From current measurements, Beardsley *et al.* (1976) have estimated the alongshore transport of shelf water (within the 100 m isobath) to be approximately 8000 km^3 $year^{-1}$. The scale given above corresponds to a uniform divergence of this transport over the length of the Middle Atlantic Bight (say, a distance of 1000 km). However Beardsley *et al.* (1976) have found similar transports at three different transects that they have measured, and the observations of Ford *et al.* (1952) and Kupferman and Garfield (1977) further suggest that the bulk of the shelf water is removed near Cape Hatteras where this southwestward drift coalesces with the Gulf Stream. We therefore suggest that F is at most $O(1)$ and is likely to be much less.

It is not realistic for the front to intersect the surface at a slanted angle. The constant wind stirring will maintain a finite-depth surface mixed layer within which the isopycnals are essentially vertical. The front cannot continue to slope toward the surface after it reaches this depth, seaward of which the alongshore current shear as well as the non-Ekman component of the offshore transport must then vanish (see Eqs. 3.12 and 3.13). This argument suggests a convergence region seaward of the frontal zone where sinking motion must occur. The sinking fluid returns shoreward underneath the frontal interface, gradually feeding into the upper layer through entrainment, thus completing the circuit. Fig. 10 shows the mean cross-shelf current in winter (averaging period is from November 1979 to March 1980) constructed from the monthly means of Beardsley *et al.* (1982), together with the mean frontal position determined by Wright (1976) from historical data. The flow direction, although consistent with the model, can also be explained by simple Ekman dynamics. A transport divergence above the front, which would be more conclusive evidence of the entrainment, cannot however be extracted from the data because of the insufficient spatial resolution. Neither is there enough spatial coverage of the array to examine the convergence region proposed by the model.

The breakdown of the model described earlier can be remedied by including some three-dimensional effects. For example, F might not be an independent parameter but vary with τ—i.e., a stronger eastward wind weakens the westward drift more rapidly, resulting in a greater offshore transport—so that it always lies within the valid domain of the model; or, the wind might set up an opposing pressure gradient that effectively reduces its effect. These complications however will introduce further arbitrariness to the model and are not particularly useful for our objective.

4. Summary and conclusions

We have presented two conceptual models of a simplified two-dimensional, two-layered frontal sys-

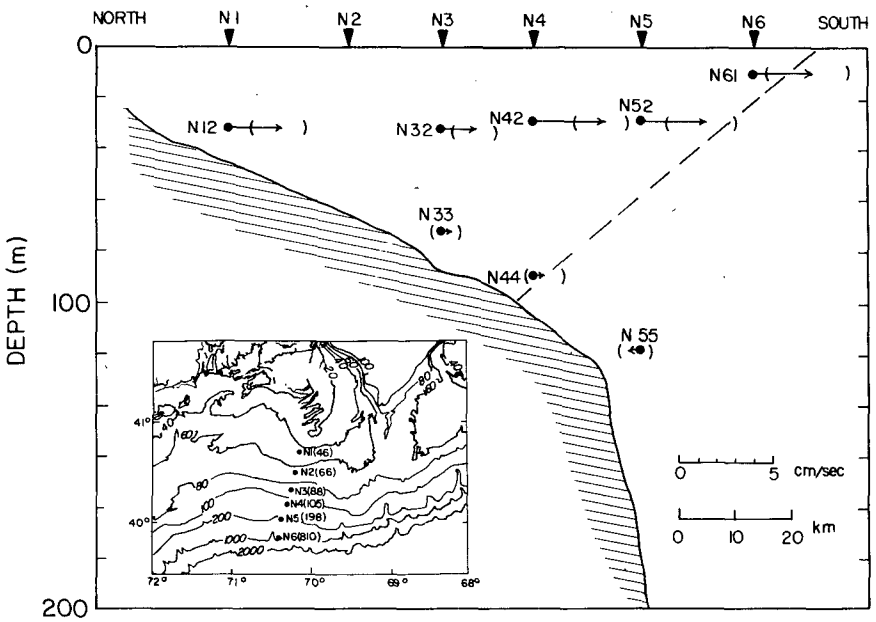

FIG. 10. Mean cross-shelf current in winter constructed from the monthly means of Beardsley *et al.* (1982). Averaging period is from November 1979 to March 1980. The brackets represent the standard error based on a correlation time scale of 5 days, and the dashed line represents the mean front (Wright, 1976) determined from historical data.

tem to study the wintertime shelf–slope front. The first model is a straightforward extension of the classical geostrophic adjustment problem to a step topography and is intended to examine the equilibrium front after the fall overturning. Being inviscid and adiabatic, it applies only over short time scales before non-conservative processes become important. The second model, on the other hand, examines the thermodynamical balance of the shelf–slope front over longer time periods when some dissipative and mixing effects are included.

From the geostrophic adjustment model, we have shown that if the shelf water is the less dense of the two water masses, then the equilibrium front over a flat bottom is little modified by the presence of a step. Despite the asymmetry of the step topography, the front retains its symmetry, and the half-width of the frontal zone, though slightly increased, is roughly given by the internal radius of deformation based on the shelf depth. In the case of dense shelf water, however, the solution shows a detached parcel of shelf water residing offshore at the bottom when the depth ratio across the step is greater than two. This predicted feature is reminiscent of some hydrographic sections made near the Weddell Sea and Ross Sea shelf breaks and the Red Sea outflow.

In the frictional model, we have demonstrated that the entrainment, although dissipative as a momentum flux, enhances the offshore transport above the front, which, when acted on by the Coriolis force, can maintain an alongfront current shear in the presence of friction. This somewhat peculiar mechanism of entrainment as a virtual momentum source works only in a rotating system and can account for the persistence of the shelf–slope front. It is further suggested that the non-Ekman component of the offshore transport sinks seaward of the frontal zone and returns shoreward to complete the circuit. There are however no adequate data to examine either the increasing offshore transport in the upper layer or its subsequent sinking as proposed by the model.

A shelf water export is postulated in the model to provide the needed buoyancy source for the steady-state thermal balance. Its buoyancy decreases offshore as the denser water is entrained upward across the frontal interface. Without wind, the buoyancy gradient varies monotonically offshore—sharpening or weakening depending on whether F, a dimensionless offshore transport, is greater or smaller than one. But with wind, an extremum can be generated. Specifically, the magnitude of the buoyancy gradient can exhibit a maximum (minimum) when wind is positive (negative). In application to the Middle Atlantic Bight where the westerlies prevail in winter and where F is O(1) or less, the model predicts the existence of an inflection point and hence a weakened buoyancy gradient above the front, much like that observed in some hydrographic data. In the lower layer, the assumption of a negligible downward entrainment leads to a uniform density field, consistent with observation.

More complicated models can certainly be constructed on the physical basis laid out here. At the present time, however, our understanding of the shelf–slope front is hampered as much by lack of sophistication in the model as by lack of adequate sampling techniques to monitor the front. Until more data are acquired that can be compared with the model, our modeling effort has to remain somewhat speculative.

Acknowledgments. I want to thank R. C. Beardsley and his collaborators for providing me information from their data report on the Nantucket Shoals Flux Experiment before its publication and R. W. Houghton for letting me use his figure. Comments from K. Brink, B. Cushman–Roisin, M. Stern and an anonymous reviewer are appreciated. I also want to thank many of my colleagues for reading and commenting on the manuscript. Support from the National Science Foundation under Grant OCE 81-17579 and the Department of Energy under Grant DEAC02-EV02185 is gratefully acknowledged.

APPENDIX A

Solution for a Wide Shelf

Solution (2.18) is obtained in the following way. Multiplying (2.12) to (2.15) by $-\cosh\gamma L$, $-\cosh\gamma R$, $\sinh\gamma L$ and $\sinh\gamma R$, respectively, adding the resulting equations, and using (2.17), we obtain

$$\sinh\gamma L - \gamma L\cosh\gamma L = \sinh\gamma R - \gamma R\cosh\gamma R,$$

which leads to

$$L = R, \tag{A1}$$

since $\sinh x - x\cosh x$ is a single-valued function of x. Similarly multiplying (2.12) to (2.15) by $-\sinh\gamma L$, $\sinh\gamma R$, $\cosh\gamma L$ and $-\cosh\gamma R$, respectively, adding them, and using (2.16) and (A1), we derive

$$\cosh\gamma L - \gamma L\sinh\gamma L = \frac{1}{2}\left(1 - \frac{1}{\delta}\right). \tag{A2}$$

A, B, $\bar{A}$, $\bar{B}$ can then be trivially solved by substituting (A1) and (A2) into the original equations.

To obtain the solution (2.22), we first notice that (A1) still holds since the equations used to derive it remain unchanged. Multiplying (2.13) and (2.15) by $\sinh\gamma R$ and $\cosh\gamma R$, respectively, and substracting the resulting equations yields

$$\gamma L\sinh\gamma L - \cosh\gamma L = \delta. \tag{A3}$$

A, B, $\bar{A}$, $\bar{B}$ can then be obtained.

APPENDIX B

Solution for a Narrow Shelf

For the case $\delta > 1$, the shelf width L is given, and all the boundary conditions, (2.7) through (2.10), ap-

ply except the one that requires $h_1 = 1$ at $y = -L$. The five equations—(2.12), (2.13) and (2.15) through (2.17)—therefore determine the five constants (A, B, $\bar{A}$, $\bar{B}$, R). Simple manipulation leads to the following solution.

$$\left.\begin{aligned} \bar{A} &= \frac{1}{\gamma^2}(\gamma R \sinh\gamma R - \cosh\gamma R) \\ A &= \bar{A} - \frac{1}{\gamma^2}\left(\frac{1}{\delta} - 1\right) \\ \bar{B} = B &= \frac{1}{\gamma^2}(\sinh\gamma R - \gamma R \cosh\gamma R) \\ \sinh\gamma(R+L) &- \gamma R \cosh\gamma(R+L) \\ &+ \gamma L + \left(\frac{1}{\delta} - 1\right)\sinh\gamma L = 0 \end{aligned}\right\} . \quad \text{(B1)}$$

The last equation relates R to L and can be solved numerically by iteration. The contours of constant R are shown in the right half of Fig. 5.

For the case $\delta < 1$, the shelf width R is given, with the requirement that $h_1 = 0$ at $y = R$, and hence (2.15) is dropped. Again the five equations—(2.12) through (2.14) and (2.16), (2.17)—determine the five constants (A, B, $\bar{A}$, $\bar{B}$, L). The solution is given by

$$\left.\begin{aligned} \bar{A} &= \frac{\delta}{\gamma^2} \\ A &= \frac{1}{\gamma^2}(\cosh\gamma L - \gamma L \sinh\gamma L) \\ \bar{B} = B &= \frac{1}{\gamma^2}(\sinh\gamma L - \gamma L \cosh\gamma L) \\ (\sinh\gamma L &- \gamma L \cosh\gamma L)\cosh\gamma R \\ &+ \gamma R + \delta \sinh\gamma R = 0 \end{aligned}\right\} . \quad \text{(B2)}$$

The last equation relates L to R, the contours of which are shown in the left half of Fig. 5.

As an example, the solution when the shelf width equals one-fifth the internal radius of deformation is shown in dashed lines in Figs. 3 and 4.

REFERENCES

Beardsley, R. C., and W. C. Boicourt, 1981: On estuarine and continental-shelf circulation in the Middle Atlantic Bight. *Evolution of Physical Oceanography,* B. A. Warren and C. Wunsch, Eds., The MIT Press, 198–233.

——, —— and D. V. Hansen, 1976: Physical oceanography of the Middle Atlantic Bight. *Middle Atlantic Continental Shelf and the New York Bight,* M. G. Gross, Ed., Amer. Soc. Limnol. Oceanogr., Special Symposia, **2,** 20–34.

——, C. A. Mills, J. A. Vermersch, W. S. Brown, N. Pettigrew, J. Irish, S. Ramp, R. Schlitz and B. Butman, 1982: Nantucket Shoals Flux Experiment (NSFE79). Part 2: Moored array data report. WHOI Ref 82 (in preparation).

Csanady, G. T., 1971: On the equilibrium shape of the thermocline in a shore zone. *J. Phys. Oceanogr.,* **1,** 263–270.

Davis, R. E., R. deSzoeke and P. Niiler, 1981: Variability in the upper ocean during MILE. Part II: Modelling the mixed layer response. *Deep-Sea Res.,* **28,** 1453–1475.

deSzoeke, R. A., and J. G. Richman, 1981: The role of wind-generated mixing in coastal upwelling. *J. Phys. Oceanogr.,* **11,** 1534–1547.

Ford, W. L., J. R. Longard and R. E. Banks, 1952: On the nature, occurrence and origin of cold low salinity water along the edge of the Gulf Stream. *J. Mar. Res.,* **11,** 281–293.

Foster, T. D., and E. C. Carmack, 1976: Frontal zone mixing and Antarctic bottom water formation in the southern Weddell Sea. *Deep-Sea Res.,* **23,** 301–317.

Griffiths, R. W., and P. F. Linden, 1982: Laboratory experiments on fronts. Part 1: Density-driven boundary currents. *Geophys. Astrophys. Fluid Dyn.,* **19,** 159–187.

Hsueh, Y., and B. Cushman-Roisin, 1982: On the formation of surface to bottom fronts over steep topography. *J. Geophys. Res.,* **88,** 743–750.

Jacobs, S. S., A. F. Amos and P. M. Bruchhausen, 1970: Ross Sea oceanography and Antarctic bottom water formation. *Deep-Sea Res.,* **17,** 935–962.

Kraus, E. G., and J. S. Turner, 1967: A one-dimensional model of the seasonal thermocline: II. The general theory and its consequences. *Tellus,* **19,** 98–106.

Kupferman, S. L., and N. Garfield, 1977: Transport of low-salinity water at the slope water–Gulf Stream boundary. *J. Geophys. Res.,* **82,** 3481–3486.

Marra, J., R. W. Houghton, D. C. Boardman and P. J. Neale, 1982: Variability in surface chlorophyll *a* at a shelf-break front. *J. Mar. Res.,* **40,** 575–591.

Mayer, D. A., D. V. Hansen and D. A. Ortman, 1979: Long-term current and temperature observations on the Middle Atlantic Shelf. *J. Geophys. Res.,* **84,** 1776–1792.

Stommel, H., and G. Veronis, 1980: Barotropic response to cooling. *J. Geophys. Res.,* **85,** 6661–6666.

Wright, W. R., 1976: The limits of shelf water south of Cape Cod, 1941 to 1972. *J. Mar. Res.,* **34,** 1–14.

Wyrtki, K., 1971: *Oceanographic Atlas of the International Indian Ocean Expedition.* National Science Foundation, Washington, D.C., 531 pp.